Journal of Cerebral Blood Flow & Metabolism (2011) 31, 819–831

www.jcbfm.com

# Brain water mobility decreases after astrocytic aquaporin-4 inhibition using RNA interference

Jérôme Badaut[1,2,3], Stephen Ashwal[1], Arash Adami[1], Beatriz Tone[1], Rebecca Recker[1], David Spagnoli[4], Béatrice Ternon[2,3] and Andre Obenaus[1,4,5,6]

[1]*Department of Pediatrics, Loma Linda University School of Medicine, Loma Linda, California, USA;* [2]*Departments of Clinical and Fundamental Neurosciences, Neurovascular Laboratory, Faculty of Medicine, Geneva University, Service of Neurosurgery, Geneva Neurosciences Centre, Geneva, Switzerland;* [3]*Neurosurgery Research Group, Lausanne Hospital University (CHUV), Lausanne, Switzerland;* [4]*Department of Radiation Medicine, Loma Linda University School of Medicine, Loma Linda, California, USA;* [5]*Department of Radiology, Loma Linda University School of Medicine, Loma Linda, California, USA;* [6]*Department of Biophysics and Bioengineering, School of Science and Technology, Loma Linda, California, USA*

**Neuroimaging with diffusion-weighted imaging is routinely used for clinical diagnosis/prognosis. Its quantitative parameter, the apparent diffusion coefficient (ADC), is thought to reflect water mobility in brain tissues. After injury, reduced ADC values are thought to be secondary to decreases in the extracellular space caused by cell swelling. However, the physiological mechanisms associated with such changes remain uncertain. Aquaporins (AQPs) facilitate water diffusion through the plasma membrane and provide a unique opportunity to examine the molecular mechanisms underlying water mobility. Because of this critical role and the recognition that brain AQP4 is distributed within astrocytic cell membranes, we hypothesized that AQP4 contributes to the regulation of water diffusion and variations in its expression would alter ADC values in normal brain. Using RNA interference in the rodent brain, we acutely knocked down AQP4 expression and observed that a 27% AQP4-specific silencing induced a 50% decrease in ADC values, without modification of tissue histology. Our results demonstrate that ADC values in normal brain are modulated by astrocytic AQP4. These findings have major clinical relevance as they suggest that imaging changes seen in acute neurologic disorders such as stroke and trauma are in part due to changes in tissue AQP4 levels.**
*Journal of Cerebral Blood Flow & Metabolism* (2011) **31,** 819–831; doi:10.1038/jcbfm.2010.163; published online 29 September 2010

**Keywords:** apparent diffusion coefficient; edema; neuroimaging; neurovascular unit; water channel

## Introduction

Water channels (aquaporins, AQPs) drive water diffusion through the plasma membrane and open new avenues for understanding the molecular underpinnings of water movement in mammalian tissues (Tait *et al*, 2008). These channels are widely distributed in several tissues, and brain AQP4 has been found to be highly expressed with a preferential location within astrocytic cell membranes in contact with blood vessels (Badaut *et al*, 2002). Several studies have already shown that AQP4 is important in edema formation and resolution after acute brain injury in various disorders, including stroke (Hirt *et al*, 2009; Tait *et al*, 2008).

*In vitro* astrocyte culture experiments have shown that AQP4 is involved in water movement within the cell membrane (Nicchia *et al*, 2003). So far, the involvement of AQP4 in cellular water mobility has not been explored *in vivo* in normal brain. The apparent diffusion coefficient (ADC) value measured using magnetic resonance imaging (MRI) represents water mobility within tissue. Water diffusion can be extracellular, intracellular, and transcellular through cell membranes, and the ADC value likely reflects all three components. Alterations of this coefficient are

Correspondence: Dr J Badaut, Department of Pediatrics, Loma Linda University School of Medicine, Loma Linda, CA 92350, USA.
E-mail: jbadaut@llu.edu
This study was supported by the Swiss Science Foundation (FN 3100AO-108001, 31003A-122166, and IZK0Z3-128973), and supported in part by the NIH R01HD061946, Pediatric Research Fund, Department of Pediatrics, and a NASA Cooperative Agreement NCC9-149 to the Radiobiology Program, Department of Radiation Medicine at Loma Linda University.
Received 25 March 2010; revised 16 August 2010; accepted 24 August 2010; published online 29 September 2010

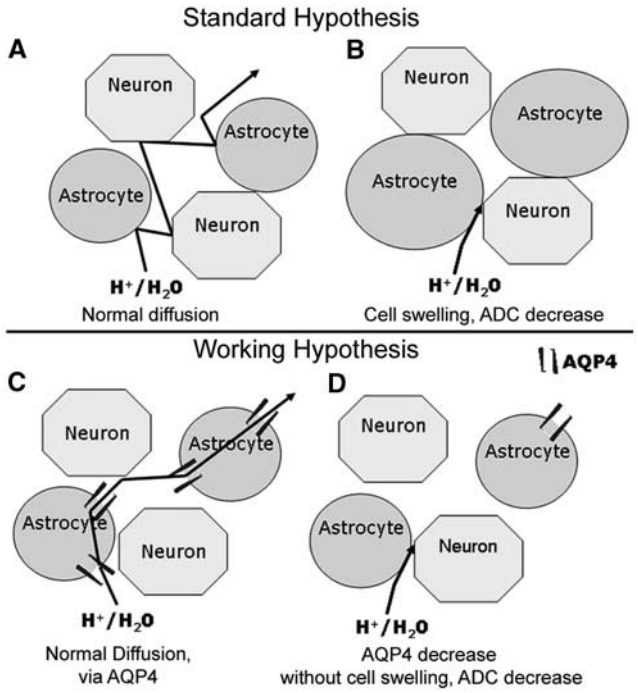


**Figure 1** Hypothesis for apparent diffusion coefficient (ADC) value changes in brain tissue. Schema depicting the standard (**A**, **B**) and our working hypothesis (**C**, **D**) to explain decreased brain ADC values following silencing of AQP4 expression. Classically, decreased ADC is associated with decreased extracellular space due to cellular swelling (**B**). The water channel, AQP4, is expressed in astrocyte membranes and can facilitate water movement (**C**). After silencing APQ4, we hypothesize that lower ADC values are caused by decreased water permeability due to a decreased number of AQP4 channels (**D**).

often used as an early indicator of ischemic injury (Obenaus and Ashwal, 2008). MRI is used for the clinical evaluation and assessment of treatment in many neurologic disorders and more recently as an early indicator of brain activation during functional MRI studies (Le Bihan, 2007).

In pathological conditions, ADC values represent water movement within tissues and reduced values are thought to be associated with decreases in the extracellular space caused by cell swelling (Figure 1). This interpretation is hypothetical and the underlying physiological basis of the ADC remains incompletely understood (Obenaus and Ashwal, 2008). A correlation between the ADC changes and AQP4 expression has been observed in rat models of hypoxic ischemic (Meng *et al*, 2004) and hydrocephalus (Tourdias *et al*, 2009). These results suggest indirectly that ADC values are correlated to the level of AQP4 expression under pathological conditions. Therefore, we hypothesized that AQP4 in astrocytes contributes significantly to water diffusion and ADC values in normal brain tissues (Figure 1). This hypothesis has never been directly tested in normal brain, and to address this question, we used RNA interference, to acutely knockdown AQP4 expression in the rat brain and evaluated brain ADC changes (Figure 1).

## Materials and methods

*In vitro* experiments described in the present work were approved by the Animal Care and Use Committee of the University of Lausanne. *In vivo* animal studies were conducted according to the principles and procedures of the Guidelines for Care and Use of Experimental Animals and were approved by Loma Linda University.

### Astrocyte Cultures and Small Interference RNA Tests

Neurospheres were prepared with striatopallidum structures from E14 mouse embryos as previously described (Brunet *et al*, 2004). Cells spontaneously formed floating neurospheres. Passages were performed at 7-day intervals by mechanical dissociation and replating at 50,000 cells per mL in new DN1 medium containing 20 ng/mL of epidermal growth factor. After mechanical dissociation of the neurospheres, cells were plated into 12-well tissue culture plates (Costar 3524, Corning, NY, USA) for differentiation into astrocytes using fetal calf serum (10%) that was added to the culture 4 days before cellular characterization and use in small interference RNA (siRNA) applications. Glial fibrillary acid protein (GFAP) staining demonstrated a pure astrocyte culture with the same metabolic properties as described in primary astrocyte cultures (Brunet *et al*, 2004).

Our AQP4 silencing protocol was adapted from a previous publication (Saadoun *et al*, 2005): custom SMART pool containing four small interference RNA duplexes against AQP4 (20 nmol/L, siAQP4, Dharmacon Research) were mixed with Dharmafect (Dharmacon Research), diluted 1:50 in Opti-MEM (Invitrogen, Basel, Switzerland). For controls, nontargeted siRNA (siGLO RNA-induced silencing complex (RISC)-free control siRNA) were used to monitor nonspecific effects of the siRNA. siGLO was prepared using the same protocol used for siAQP4. The mixture was incubated for 20 minutes at room temperature for complex formation and then added to the cells. For each experiment, specific silencing was confirmed by Western blot and dot blot analysis 4 days after transfection.

Sequences of siAQP4 in the SMART pool were submitted to a BLAST search to avoid the possible targeting of other genes present in brain. The four individual siRNA duplexes against AQP4 present in the SMART pool were tested individually on astrocyte cultures and gave the same degree of inhibition (data not shown).

### Organotypic Slice Cultures and Small Interference RNA Tests

Organotypic hippocampal slice cultures were prepared as previously described (Badaut *et al*, 2005; Hirt *et al*, 2004). Briefly, coronal hippocampal sections (350 $\mu$m) were dissected from 10- to 12-day-old rats (Sprague-Dawley, Charles River, Arbresle, France) and placed onto sterile porous membrane units (Millicell-CM, Millipore, Billerica,

MA, USA) in wells containing 1 mL of culture medium with 25% horse serum, 50% minimal essential medium supplemented with HEPES and sodium bicarbonate, 25% Hank's salt solution, L-glutamine (2 mmol/L), and D-glucose (35 mmol/L). Cultures were grown at 33°C, 100% humidity, 5% $CO_2$ for 7 days, an then transferred to culture medium with 15% horse serum, containing D-glucose (5 mmol/L), which was changed every 3 to 4 days.

For slice cultures, we modified the protocol used for astrocyte cultures to improve transfection and silencing. SMART pool siRNA duplexes against AQP4 (400 ng, siAQP4, Dharmacon Research) and siGLO (400 ng, Dharmacon Research) were mixed with 2 $\mu$L of interferin (Polyplus-transfection, Illkirch, France), diluted in a saline solution (0.9%) containing 5% glucose for final volume of 4 $\mu$L. The reagents were incubated for 20 minutes at room temperature for complex formation and then 4 $\mu$L were dispensed onto the CA1 area. AQP4 protein expression was determined by immunoblotting after 3 and 4 days after application of siGLO or siAQP4 (see protocol below, $n=4$ independent experiments with eight slices/condition). Immunohistochemistry was also performed on fixed slices with 4% paraformaldehyde in phosphate-buffered saline (PBS) ($n=4$ independent cultures with four slices). The adapted transfection protocol developed for slice cultures was used for the *in vivo* experiments.

## Rat Surgery and Small Interference RNA Injection

Male Sprague–Dawley rats (Charles River, San Diego, CA, USA) were used at P17 ($n=22$). Rats were housed in individual plastic cages in a room with controlled temperature and a light cycle from 0600 to 1800 hours and acclimatized for 7 days with food and water provided *ad libitum*.

For intracortical injection, rats were anesthetized with 3% isoflurane and placed in a stereotaxic apparatus (David Kopf Instrument, Tujunga, CA, USA). A sterile 22-gauge needle on a Hamilton syringe for injection into the right frontal cortex with coordinates of 0.0 mm posterior to the bregma, 1.0 mm lateral to the midline, and 1.0 mm to the surface of the skull (Supplementary Figure 1). The siRNA mixture was prepared as described for the organotypic slice cultures (see above). The 4 $\mu$L of mixture were injected into the cortex at 0.4 $\mu$L/min, with a second injection repeated 2 days later (Supplementary Figure 1). For regional and cellular distribution of siRNA in the brain, untargeted siRNA (siGLO) tagged with the fluorescent dye, CY3 (CY3-siGLO) was used 3 days after the initial siRNA injection. Rat brains were freshly collected ($n=4$) and frozen for protein analysis and other rats ($n=7$) were transcardially perfused with 4% paraformaldehyde for immunohistochemistry.

## Magnetic Resonance Imaging Experiments and Analysis

The MRI was performed at 3 days after siRNA and siGLO injection ($n=4$, per group). Rats were lightly anesthetized using isoflurane (1.0%) and then imaged on a Bruker Avance 11.7 T MRI (Bruker Biospin, Billerica, MA, USA) (Badaut *et al*, 2007; Obenaus *et al*, 2007). Two imaging data sets were acquired: (1) a 10 echo T2 and (2) a diffusion-weighted sequence, where each sequence collected 20 coronal slices (1 mm thickness and interleaved by a 1 mm). The T2 sequence had the following parameters: TR/TE (time to repetition/echo time) = 4,600 milliseconds/10.2 milliseconds, matrix = 128 × 128, field of view = 3 cm, NEX (number of acquisitions) = 2 and acquisition time = 20 minutes. The spin echo diffusion sequence parameters were TR/TE = 3,000 milliseconds/25 milliseconds, *b* values = 0.72, 1,855.64 s/mm$^2$, matrix = 128 × 128, field of view = 3 cm, NEX = 2, and acquisition time = 25 minutes.

T2 and ADC values were quantified using standardized protocols published previously (Badaut *et al*, 2007; Obenaus *et al*, 2007) on a single coronal slice (1 mm thick) at the site of the injection (Figure 7A) and at the same level used for histology analysis. T2 maps were generated and ADC maps were calculated using a linear two-point fit. Four primary regions of interest (ROIs) within ipsi- and contralateral hemispheres (cortex and striatum) were delineated on T2WI with ipsi-cortex (23 pixels); contra-cortex (40 pixels); ipsi and contra striatum (41 pixels each) (Supplementary Figure 1). These ROIs were overlaid onto corresponding T2 and ADC maps and the mean, s.d., number of pixels and area for each ROI were extracted. The MRI analysis was performed by two masked readers without knowledge of treatment. The difference in the results obtained by the two readers was 2% in siGlo-treated animals and 7% variability in the siAQP4-treated animals.

## Western Blot Analysis

After imaging, four animals were freshly dissected and seven were transcardially perfused with 4% paraformaldehyde. The freshly dissected brains were frozen and cut at −20°C on a cryostat (Leica, Glattbrugg, Switzerland). Quantification of AQP4 Western blots was performed as previously described (Hirt *et al*, 2009). Protein was prepared from tissues slices obtained from frozen brains of siGLO- and siAQP4-treated rats. Slices were prepared in an appropriate buffer (Hirt *et al*, 2009) and sonicated for 30 seconds. A measure of 1 $\mu$g of protein was then subjected to SDS polyacrylamide gel electrophoresis on a 12% gel (Nupage, Invitrogen, Carlsbad, CA, USA) for the quantification of AQP4. Proteins were then transferred to a polyvinylidene fluoride membrane (PerkinElmer, Schwerzenbach, Switzerland). The blot was incubated with a polyclonal antibody against AQP4 (Chemicon, Temecula, CA, USA, 1:3,000) and a monoclonal antibody against actin (Sigma, Buchs, Switzerland, 1:25,000) in Odyssey blocking buffer (LI-COR Bioscience, Lincoln, NE, USA) overnight at 4°C. After washing, the filter was incubated with two fluorescence-coupled secondary antibodies (1:10,000, anti-rabbit Alexa-Fluor-680 nm, Molecular Probes, Oregon (Eugene, OR, USA) and anti-mouse immunoreactivity (IR)-Dye-800 nm, Roche, Basel, Switzerland) for 2 hours at room temperature. After washing, the degree of fluorescence was measured using an infrared scanner (Odyssey, LI-COR Bioscience, Lincoln, NE, USA).

Quantification was performed blindly by two experimenters (J.B. and B.T.) for total AQP4 (Hirt *et al*, 2009).

### Immunohistochemistry and Image Analysis

The fixed brains were put in 30% sucrose in PBS for cryoprotection before freezing and cutting on a cryostat.

*IgG staining for blood–brain barrier evaluation*: Sections were incubated for 4 hours at room temperature with biotin-conjugated affinity purified donkey anti-rat IgG coupled with biotin (Vector Laboratories, Burlingame, CA, USA, 1:200) and then a streptavydin-coupled infrared-dye-680 nm (Molecular Probes) diluted (1:400) in PBS containing 0.1% Triton X-100 and 1% bovine serum albumin. After washing, sections were scanned on an Odyssey infrared scanner to quantify fluorescence in ROI (same as defined in MRI experiments) on two adjacent slices. The IR was quantified and fluorescence was converted into average integrated intensities from the ipsilateral and contralateral hemispheres. The integrated intensities were expressed as a percent of values from control rats.

*AQP4/GFAP/NeuN immunohistochemistry*: Commercially available, affinity purified, rabbit polyclonal antibodies were used for AQP4 and GFAP immunolabeling (Chemicon International, Temecula, CA, USA), and mouse monoclonal antibodies were used for GFAP and neuronal nuclei (NeuN) (Chemicon International) labeling. Immunostaining was performed in PBS containing 0.1% Triton X-100 and 0.3% bovine serum albumin and after each incubation sections were rinsed in PBS $3 \times 10$ minutes.

For immunolabeling, sections were first incubated overnight at 4°C with anti-AQP4 (1:300), GFAP (1:400), and NeuN (1:500). After washing, floating sections were incubated for 2 hours at room temperature with secondary antibodies.

Infrared immunofluorescence was performed for AQP4 and GFAP staining using secondary antibodies containing an infrared-dye-680-nm secondary anti-rabbit (1:1,000, Molecular Probes) and an infrared-dye-800-nm secondary anti-rabbit (1:1,000, Roche) antibody. Sections were scanned with an Odyssey infrared scanner and fluorescence was quantified (Badaut *et al*, 2007). The fluorescence from AQP4-IR and GFAP-IR were quantified with four ROIs placed in ipsilateral and contralateral cortices and striatum.

In a second set of experiment, Alexa-Fluor-594 nm coupled secondary rabbit antibody (Molecular Probes, Invitrogen, 1:500) and Alexa-Fluor-468 nm coupled secondary mouse antibody (Molecular Probes, Invitrogen, 1:500) were used to reveal anti-AQP4, anti-GFAP, and anti-NeuN. Sections were mounted and coverslipped with anti-fading medium Vectashield containing DAPI (Blue color in pictures, Vector, Vector laboratories). Immunofluorescent preparations were examined using confocal laser scanning microscopy (Zeiss, Feldbach, Switzerland) and epifluorescence microscopy (Olympus, BX41, Switzerland). Optical density measurements of AQP4 immunoreactivity was performed using Morpho-Expert (Explora-Nova, La Rochelle, France) on 1 $\mu$m thick confocal laser scanning microscopy images at three different levels in each slice and in three different regions of the ipsilateral and contralateral cortex and striatum. All measurements were performed by two masked experimenters (J.B., B.T.) on raw images from four independent series of immunohistochemical experiments. This method of quantification showed the same trends observed with infrared immunohistochemistry.

NeuN-positive cells were counted in the four selected ROIs each one containing 80 to 95 different fields ($422 \times 338\ \mu m^2$). The counting of NeuN-positive nuclei was automatically performed using Mercartor software (Explora-Nova). The accuracy of the counting was previously tested on slices from control rats stained with NeuN and DAPI, and no significant differences were observed between the two hemispheres (data not shown).

For astrocyte morphology, convexity factors were measured using Morpho-Expert (Explora-Nova) from GFAP-stained tissues. This factor was calculated using the following: convexity factor $= P_h/P_c$, where $P_h$ and $P_c$ are the perimeters of the convex hull and cell, respectively (Soltys *et al*, 2005). These values were semiautomatically calculated from binarized images from three different areas inside the ipsilateral and contralateral cortex and striatum in four independent series of immunohistochemistry experiments, using Morpho-expert (Explora-Nova).

For all immunohistochemical experiments, controls were performed by omitting the primary antibody, which gave negative results with no detectable labeling. Depletion of the AQP4 antibody by an excess of the specific peptide (Chemicon International) was also performed and gave negative results as previously observed (de Castro Ribeiro *et al*, 2006).

### Statistical Analysis

All data are presented as the mean ± s.e.m. and statistical analysis was performed using GraphPad InStat version 3.05 (GraphPad Software, San Diego, CA, USA) and (Sigmastat, SPSS Inc., Chicago, IL, USA). A Kolmogorov and Smirnov test was first performed to assess the Gaussian distribution of the data. Data that passed the test were analyzed with an unpaired *t*-test, and analysis of variance followed by Tukey–Kramer multiple comparison tests. For other data (Western blot analysis) nonparametric Wilcoxon and Kruskal–Wallis tests were used.

## Results

### *In Vitro* AQP4 Inhibition

RNA interference experiments were performed using a siRNA specifically designed against AQP4 (siAQP4) or a nontargeted siRNA (siGLO) as a control. The siAQP4 was first tested in astrocyte cultures and revealed a 76% ± 4% decrease in AQP4 compared with siGLO-treated cultures (Figure 2A), with no cellular morphologic changes (Figure 2B). Our *in vitro* results are in accordance with previous publications (Nicchia *et al*, 2005; Saadoun *et al*,

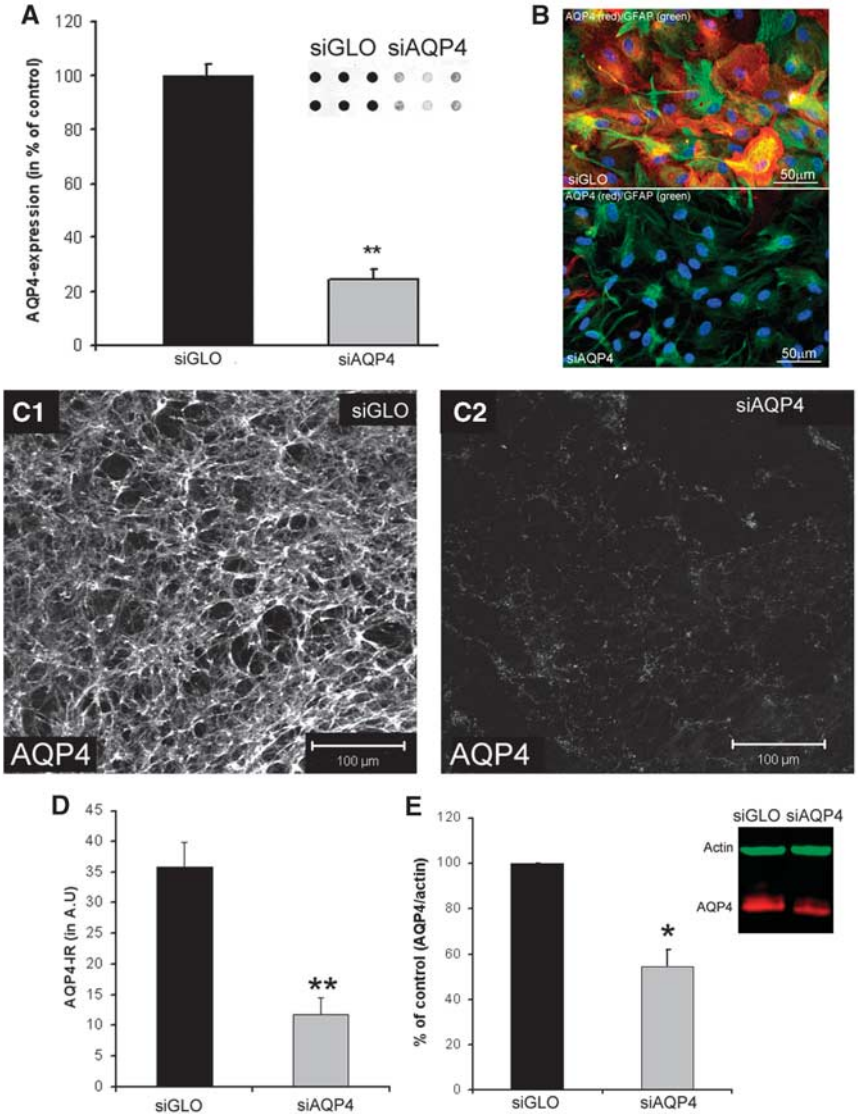


**Figure 2** *In vitro* application of small interference RNA against AQP4 (siAQP4) decreases AQP4 expression. (**A**) AQP4 expression was quantified from dot blot experiments (inset) in primary astrocyte cultures treated with siGLO (control) and siAQP4. AQP4 expression was decreased 3 days after siAQP4 application (76% ± 4%, $^{**}t$-test, $P < 0.001$, $n = 6$). (**B**) AQP4 (red) and GFAP (green) immunolabeling in primary astrocyte cultures treated with siGLO (control, $n = 6$) and siAQP4 ($n = 6$) showed no morphological differences between groups. Nuclei were stained with DAPI (blue). (**C**) Confocal images of AQP4 immunoreactivity (AQP4-ir) in CA1 of control (siGLO, **C1**) and siAQP4-treated organotypic hippocampal slices (**C2**) demonstrated a large decrease in AQP4 staining. (**D**) Optical densities of immunohistochemistry from organotypic slices showed a significant decrease in AQP4-ir from siAQP4-treated slices (67%) compared with siGLO-treated slices (analysis of variance and Tukey–Kramer multiple comparisons tests, $^{**}P < 0.001$, $n = 8$). These results provided the basis for our small interference RNA (siRNA) transfection protocol for *in vivo* experiments. (**E**) AQP4 expression quantified from Western blot experiments (inset) in organotypic hippocampal slice cultures treated with siGLO (control), or siAQP4. Treatment with siAQP4 decreased AQP4 levels (inset: red) (54% ± 7%) compared with siGLO-treated (i.e., control) hippocampal slices (Kruskal–Wallis test, nonparametric analysis of variance, $^{*}P < 0.05$, $n = 6$). GFAP, glial fibrillary acid protein.

2005). The maximum decrease in AQP4 expression was observed at 3 days after siRNA application (Supplementary Figures 2A and 2B). An adapted protocol for siAQP4 used *in vivo* was validated on hippocampal slice cultures, demonstrating a significant decrease in AQP4 expression at 3 days in astrocytes by Western blot (54% ± 7% of control, Figure 2E) and immunohistochemistry (67% of control, Figures 2C and 2D).

### *In Vivo* Small Interference RNA Diffusion and Cell Transfection

Injection of siGLO tagged with CY3, a fluorescent dye, showed diffusion of siRNA along the corpus callosum, into the contralateral cortex and bilaterally into the striatum (Figures 3A and 3B). Astrocytes were positively transfected by siAQP4 as demonstrated by the presence of CY3 fluorescence in

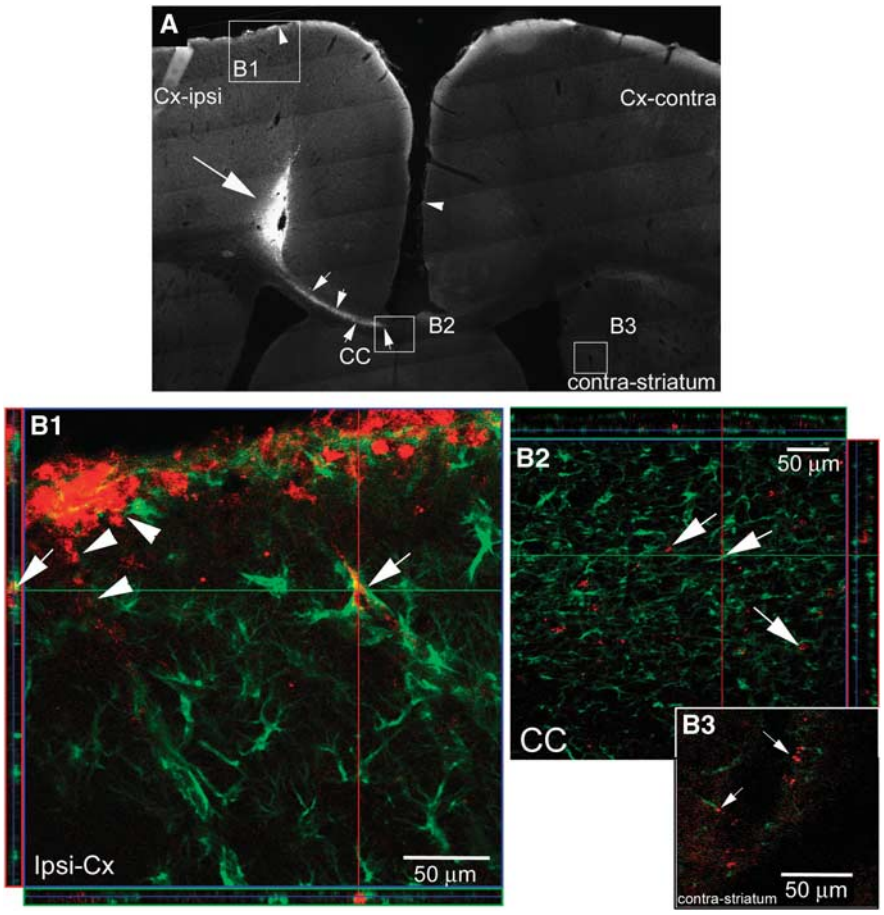


**Figure 3** Small interference RNA (siRNA) for AQP4 diffuses within brain tissues. (**A**) Diffusion of nontargeted siRNA (siGLO) tagged with CY3 in a rat coronal section at the site of injection. CY3-siGLO (large arrow) was observed in the cortex at the site of injection and siRNA diffused within the brain parenchyma toward the contralateral striatum via the corpus callosum (CC, small arrows and inset box, higher magnification **B2**). The presence of siRNA was also detected at the surface (**B1**) of the ipsilateral and contralateral cortex (arrow heads) and within the ipsilateral striatum (not shown). (**B**) Confocal images (**B1**, **B2**, **B3**) of GFAP (green) and siGLO-CY3 (red) immunostaining at 3 days after the initial injection. (**B1**) Double staining revealed positive CY3 in astrocytes (arrows) around blood vessels and also in the glia limitans (arrowheads) in close proximity to the injection site. Several astrocytes were transfected by the tagged siRNA. (**B2**) In the CC, siRNA was detected in astrocytes (arrows), showing that the siRNA is able to diffuse via the CC to the contralateral hemisphere. (**B3**) Far from the injection site, siGLO-CY3 was observed in astrocytes in contact with blood vessels (arrows) within the contralateral striatum. GFAP, glial fibrillary acid protein.

GFAP-positive cells (Figure 3B). This protocol allowed us to study siAQP4 effects on brain areas remote from the injection site (Figures 3A and 3B) including the contralateral striatum (Figure 3B3).

### AQP4 Expression After Small Interference RNA Against AQP4

Western blot analysis of the ipsilateral brain hemisphere showed that AQP4 expression was decreased by 27% in siAQP4-treated rats compared with controls ($1.23 \pm 0.11$ in control versus $0.90 \pm 0.09$ in siAQP4, $P < 0.05$. unpaired *t*-test, Figures 4A and 4B).

AQP4 isoforms, AQP4-m1, and AQP4-m23, were both decreased after injection of siAQP4 in our experiments (Supplementary Figure 3).

Immunohistochemistry demonstrated that perivascular AQP4 expression was decreased in the ipsilateral cortex adjacent to the site of injection (Figures 4C1, 4C2, and 4E). In the contralateral striatum (Figure 4D), AQP4 staining was also significantly decreased compared with siGLO ($11.4 \pm 1.9$ versus $18.6 \pm 1.5$, $P < 0.01$, unpaired *t*-test, Figures 4D1, D2, and 4E). A decrease in AQP4 staining was observed on the astrocyte endfeet in contact with blood vessels, in the neuropil and in the glia limitans (Figures 4C and 4D; Supplementary Figure 4). Interestingly, the level of AQP4 expression in cells lining the third ventricle was not changed (Supplementary Figures 4G and 4H).

### Morphological Tissue Analysis

Several histological and morphological analyses were undertaken to demonstrate that decreased

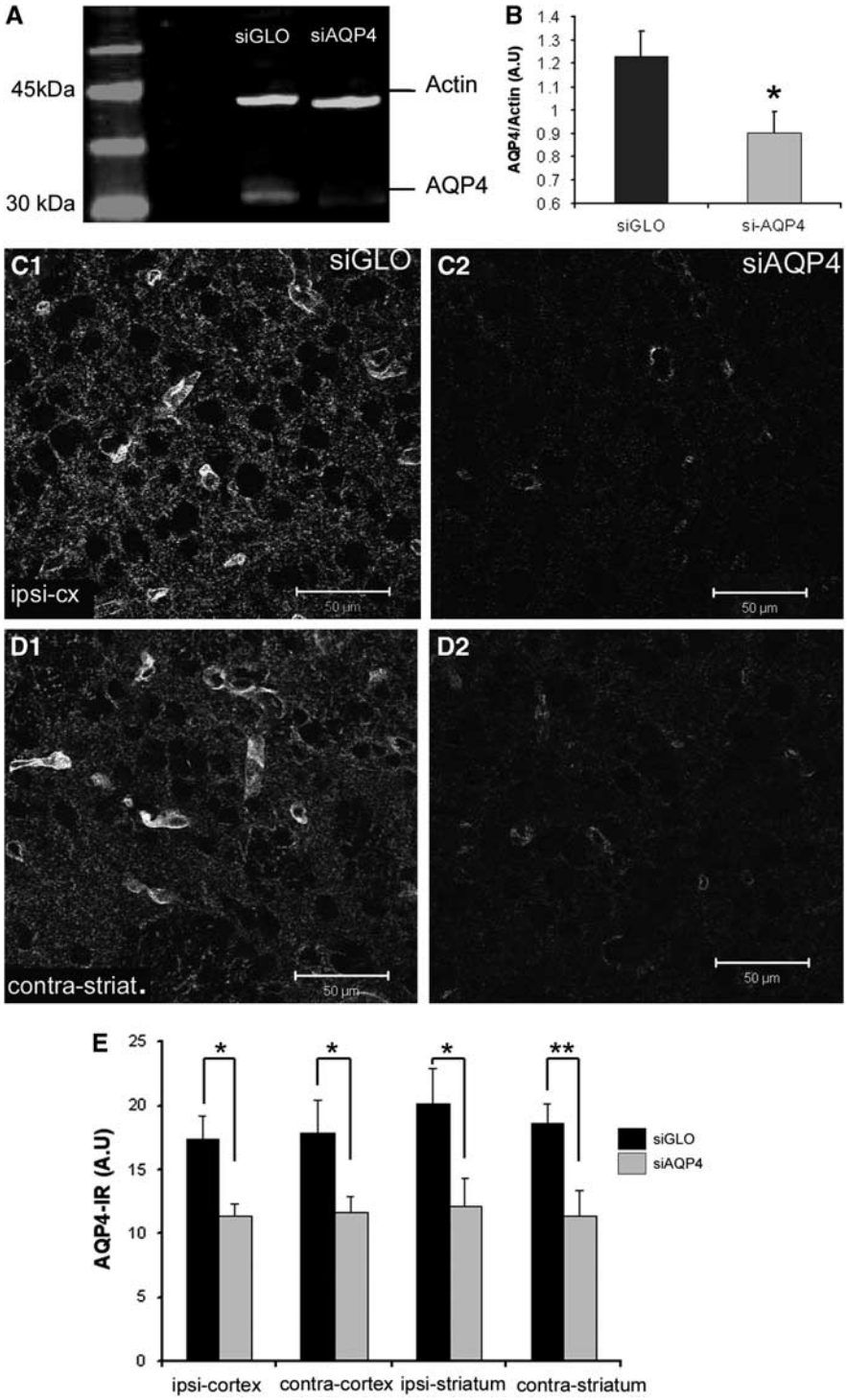


**Figure 4** Efficiency of AQP4 inhibition with small interference RNA against AQP4 (siAQP4). (**A**) AQP4 expression in siGLO- and siAQP4-treated rats was analyzed by Western blot where a specific band at 30 kDa was observed (red) in siGLO-treated rats. The intensity of the signal was decreased in siAQP4-treated rats, with no change in the intensity of the actin band (green). (**B**) Expression of AQP4 ($n = 4$) was decreased ($0.9 \pm 0.09$ arbitrary units, A.U.) in siAQP4 compared with siGLO-treated animals ($1.22 \pm 0.11$ A.U., $^*P < 0.05$, unpaired *t*-test). (**C**) AQP4 immunolabeling was also performed to examine variations in AQP4 expression *in situ*. (**C1**, **C2**) Confocal images of AQP4 staining in siGLO- (**C1**) and siAQP4 (**C2**)-treated rats showed a significant decrease in the intensity of AQP4 staining in the ipsilateral cortex of siAQP4-treated rats ($P < 0.05$, unpaired *t*-test). (**D**) AQP4 labeling in the contralateral striatum of the siGLO- (**D1**) and siAQP4-treated rats (**D2**) revealed decreased AQP4 expression. These immunohistochemical results are in accordance with the Western blot decreases in AQP4 expression (Figures 2A and 2B). (**E**) AQP4 immunolabeling ($n = 6$) was quantified using optical densitometry demonstrating a decrease in all brain areas ($^*P < 0.05$ and $^{**}P < 0.001$, unpaired *t*-test). The color reproduction of this figure is available on the html full text version of the manuscript.

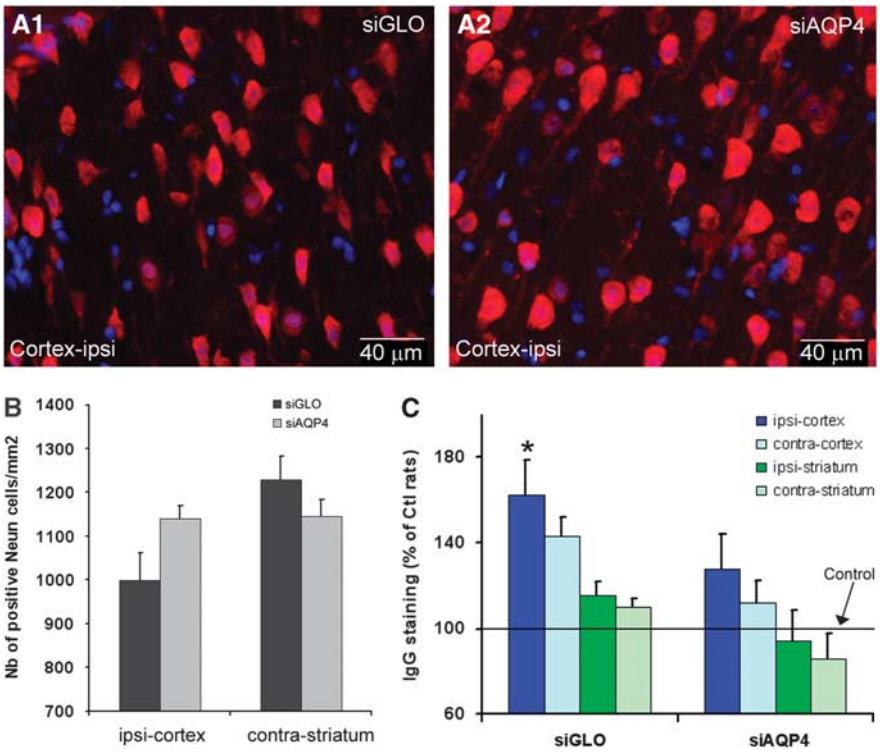


**Figure 5** Effects of small interference RNA against AQP4 (siAQP4) injection on neuronal survival and blood–brain barrier (BBB) integrity. (**A**) Neuronal changes were evaluated using NeuN (red) immunolabeling and counterstained with DAPI staining for cell nuclei (blue) in the ipsilateral cortex of siGLO- (**A1**) and siAQP4 (**A2**)-treated rats. (**B**) The number of NeuN-positive cells in four different regions of interest (ROIs) was not significantly altered in the siAQP4-treated compared with the siGLO-treated rats (analysis of variance, $n = 5$ rats). In ipsi-cortex, the number of neurons in siAQP4-treated rats ($1{,}139 \pm 30$ neurons per $mm^2$) was higher than in the siGLO rats ($998 \pm 62$ neurons per $mm^2$, analysis of variance, $P = 0.4$). Similarly, no significant results were seen in the contralateral striatum ($1{,}145 \pm 38$ neurons per $mm^2$) of siAQP4-treated versus siGLO-treated rats ($1{,}229 \pm 53$ neurons per $mm^2$, analysis of variance, $P = 0.2$). The data are consistent with the idea that siAQP4 is not toxic in brain regions where small interference RNA (siRNA) is detected. (**C**) IgG staining was used to evaluate BBB integrity 3 days after siGLO and siAQP4 injection in four ROIs (ipsilateral and contralateral cortex and striatum). In siGLO-treated rats, IgG staining was increased within the ipsilateral cortex ($162\% \pm 16\%$, analysis of variance and Tukey–Kramer multiple comparisons tests, $^*P < 0.05$, $n = 5$) compared with controls and siAQP4-treated rats ($128\% \pm 16\%$). In the other ROIs, there were no significant modifications of IgG staining compared with control values suggesting that the BBB was not affected.

AQP4 levels were not due to altered tissue composition. In the ipsilateral cortex close to the needle track, there was no significant difference in the number of neurons in siAQP4-treated ($1{,}139 \pm 30$ per $mm^2$) compared with siGLO-treated rats ($998 \pm 62$ per $mm^2$, Figures 5A and 5B), suggesting that silencing AQP4 is not toxic to neurons. In the ispilateral cortex, astrocyte staining (anti-GFAP) revealed that gliosis formation due to insertion of the needle was reduced 58.3% in siAQP4-treated rats compared with siGLO controls ($P < 0.05$, analysis of variance, Tukey–Kramer tests, Figures 6A1, A2, and 6C). Increased IgG staining in the ipsilateral cortex of siGLO-treated rats (Figure 5C) was consistent with needle track induced blood–brain barrier (BBB) disruption, but increased IgG staining was not observed in siAQP4-treated rats (Figure 5C). These results suggest that BBB disruption was minimized in the siAQP4-treated animals at the site of the injection compared with siGLO-treated rats (Figure 5C), a finding that correlates well with our observed lack of gliosis (Figures 6A1, A2, and 6C).

One important observation was that AQP4 expression was decreased at sites distant from the site of injection (ipsilateral striatum and contralateral cortex and striatum, Figure 4). In the contralateral striatum, the neuronal count showed no difference between siAQP4- ($1{,}145 \pm 38$ per $mm^2$) and siGLO-treated animals ($1{,}229 \pm 53$ per $mm^2$) (Figure 5B). Astrocytic GFAP expression was also not significantly altered in the contralateral striatum in siAQP4 rats compared with siGLO (Figures 6B1, B2, 6C, and 6D). Similarly, astrocyte morphology showed no difference between the groups (Figures 6A–6D). Together, these results demonstrate that AQP4 silencing did not affect astrocyte morphology, identical to our *in vitro* studies (Figure 2B).

### Reduced AQP4 Expression Elicits Decreased Apparent Diffusion Coefficient Values

Acute AQP4 silencing resulted in a significant decrease in ADC values bilaterally within the cortex

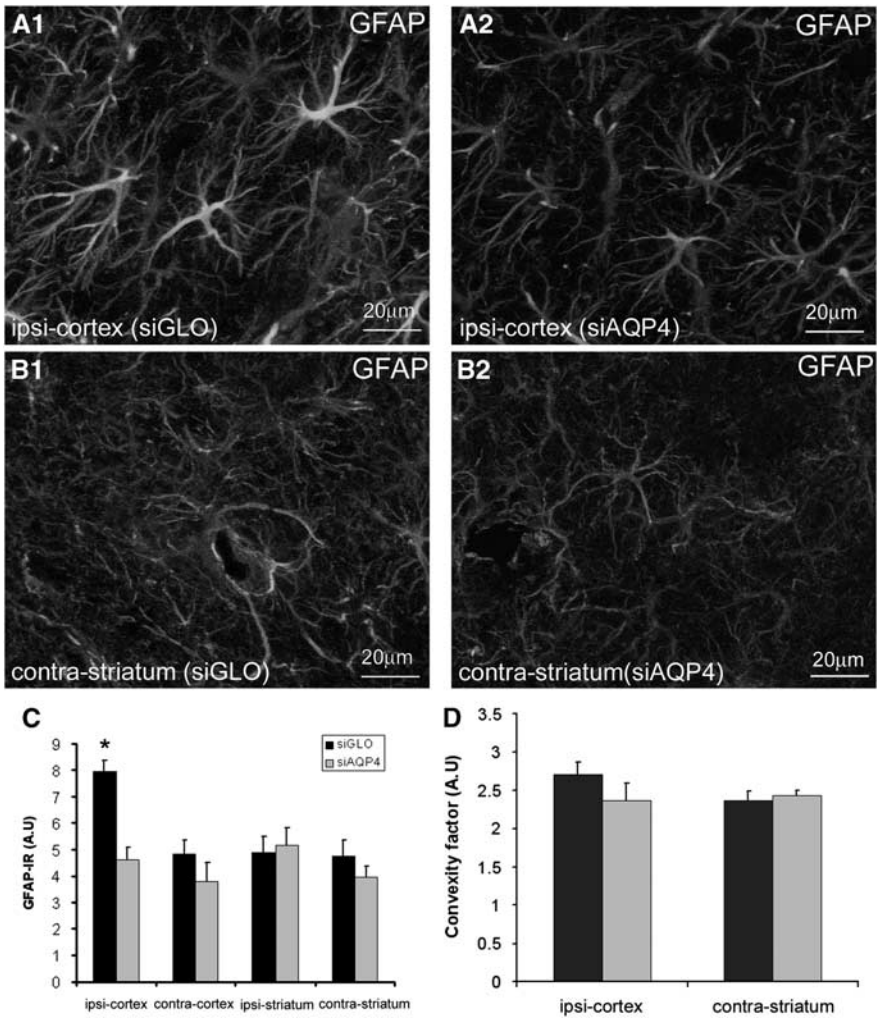


**Figure 6** Small interference RNA against AQP4 (siAQP4) has no effect on astrocyte morphology. (**A**, **B**) Astrocyte morphology using GFAP staining following AQP4 silencing was evaluated in animals undergoing neuroimaging. GFAP staining was examined in siGLO-treated rats (**A1**, **B1**) and in siAQP4-treated rats (**A2**, **B2**) in the ipsilateral cortex adjacent to the injection site (**A1**, **A2**) and in contralateral striatum (**B1**, **B2**). There was increased GFAP staining intensity in siGLO-treated (**A1**) compared with siAQP4-treated rats (**A2**) in the ipsilateral cortex, that was confirmed by of fluorescence quantification (**C**). In the contralateral striatum (contra-striatum), GFAP staining in siGLO-treated rats (**B1**) and in siAQP4-treated rats (**B2**) showed no differences in staining intensity. The presence of siAQP4 did not significantly affect the morphology of the astrocytes in the ipsilateral cortex (**A1**, **A2**) or contralateral cortex (**B1**, **B2**). (**C**) Quantification of GFAP-IR showed a significant increase in the ispilateral cortex (ipsi-cortex) of the siGLO-treated rats ($7.95 \pm 0.40$ A.U.) compared with the siAQP4-treated rats ($4.63 \pm 0.43$ A.U., analysis of variance and Tukey–Kramer multiple comparisons tests, $^*P < 0.05$, $n = 7$) demonstrating that siAQP4 prevents an increase in GFAP expression. (**D**) Astrocyte morphology was quantified using convexity factor and demonstrated that the presence of siAQP4 did not affect astrocyte morphology identical to our *in vitro* results. GFAP, glial fibrillary acid protein; IR, immunoreactivity.

and striatum, and at distance from the site of injection in an anterior to posterior direction (Figure 7). In the ipsilateral cortex at the site of injection, ADC values were decreased 33% after siAQP4 ($60.8 \pm 2.5 \times 10^{-5}\,mm^2/s$) compared with si-Glo-treated controls ($91.1 \pm 2.5 \times 10^{-5}\,mm^2/s$; $P < 0.05$, analysis of variance and Tukey–Kramer multiple comparison test) (Figures 7A and 7C). Decreased ADC values were also observed in the ipsilateral striatum (51%) and contralateral cortex (51%) and contralateral striatum (50%) compared with siGLO animals. In contralateral striatum, ADC values were decreased 51% (siAQP4, $45.4 \pm 1.7 \times 10^{-5}\,mm^2/s$; siGlo, $92.1 \pm 1.0 \times 10^{-5}\,mm^2/s$, $P < 0.01$, analysis of variance and Tukey–Kramer multiple comparison test) (Figure 7C). At 1 and 2 days after siAQP4 injection, the ADC values were not significantly altered (Supplementary Figure 5A) and water content was also unchanged (Supplementary Figure 5B). Water content, based on T2-weighted images, showed no changes at 3 days (Figures 7B and 7D).

## Discussion

The principal novel finding of the current study is that silencing AQP4 expression resulted in a decrease in water mobility, as measured using

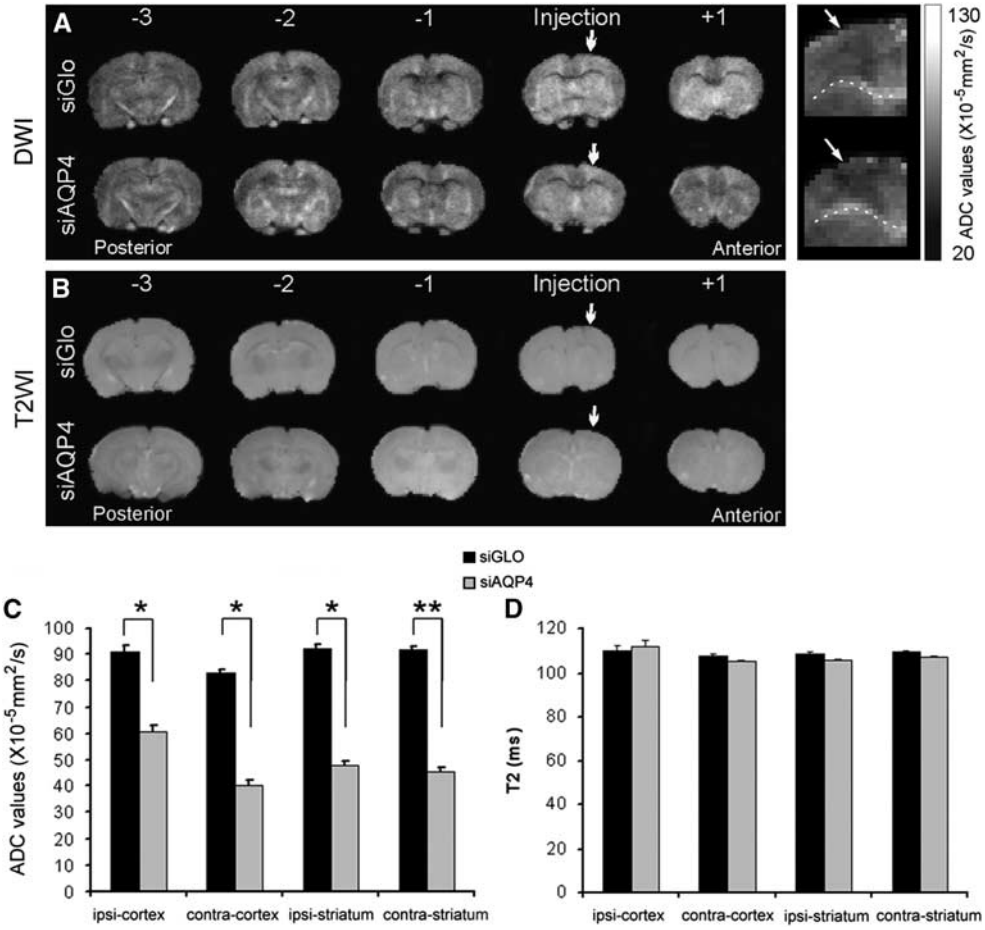


**Figure 7** Apparent diffusion coefficient (ADC) and T2 values after small interference RNA against AQP4 (siAQP4) injection. (**A**) The *in vivo* ADC was calculated in siGLO- and siAQP4-treated rats from anterior to posterior brain regions. A global decrease in ADC values was observed at several levels ( + 1, injection, −1, −2, −3). Enlarged ADC images focusing on the contra-cortex showed a decrease in ADC in siAQP4 compared with siGLO-treated rats (right panel). Arrows illustrate decreased ADC location in the cortex (dotted line indicates corpus callosum). The quantification of the ADC was performed at the site of injection at the same level used for the histology. (**B**) The *in vivo* T2 was recorded in siGLO- and siAQP4-treated rats from anterior to posterior brain regions. No changes were observed within the brains of both groups. (**C**) In the ipsilateral cortex (ipsi-cortex), ADC values in siAQP4-treated rats were significantly decreased to $60.8 \pm 2.5$ compared with $91.1 \pm 2.5 \times 10^{-5}\,mm^2/s$ in siGlo rats representing a 33% reduction ($^*P < 0.05$, analysis of variance and Tukey–Kramer multiple comparison test, $n = 4$). Similarly, a 50% decrease was observed in ipsilateral striatum and in contralateral cortex and striatum. In the contralateral striatum, ADC values were $45.4 \pm 1.7$ in siAQP4-treated rats compared with $92.1 \pm 1.0 \times 10^{-5}\,mm^2/s$ in siGLO representing 51% decrease ($^{**}P < 0.01$, analysis of variance and Tukey–Kramer multiple comparison test). (**D**) T2 values, measured in siGLO- and siAQP4-treated rats were not significantly different between brain regions suggesting that water content was not changed.

MRI-derived ADC values in normal brain tissue. Our results strongly suggest that astrocytes, and in particular their water channels, greatly contribute to water mobility.

Until now, the contribution of brain AQP4 to water movement has primarily been shown in astrocyte cultures prepared from wild-type mice treated with siRNA or from AQP4-knockout ($AQP4^{-/-}$) mice (Manley *et al*, 2004; Nicchia *et al*, 2003, 2005). *In vivo*, the role of AQP4 in water movement was evaluated in several pathological models using transgenic mice (Manley *et al*, 2004). AQP4 was shown to have a key but dual role in edema formation and resolution (Tait *et al*, 2008). Using transgenic mice lacking AQP4 ($AQP4^{-/-}$), the authors showed that AQP4 aggravated cytotoxic edema formation (Manley *et al*, 2000) and likewise facilitated water removal in vasogenic edema (Papadopoulos *et al*, 2004). Alternative existing mouse models have also been used to study the role of AQP4, including the dystrophin null mdx-$\beta$ transgenic mouse (mdx) and the $\alpha$-syntrophin null mouse ($Syn^{-/-}$) (Amiry-Moghaddam *et al*, 2003; Nico *et al*, 2003; Vajda *et al*, 2002). These transgenic mice have a normal AQP4 protein level but a significant reduction in AQP4 expression in the astrocytic foot processes surrounding blood vessels and at the glia limitans (Amiry-Moghaddam *et al*, 2003; Nico *et al*, 2003; Vajda *et al*, 2002). These previous experiments have confirmed that AQP4 has an

important role in cytotoxic edema formation in water intoxication and stroke models (Amiry-Moghaddam *et al*, 2004; Vajda *et al*, 2002).

Under normal physiological conditions, Manley *et al* (2004) reported that brains from wild-type and AQP4$^{-/-}$ mice did not reveal gross anatomical differences by light microscopy and structural MRI. However, the extracellular space was increased in the AQP4$^{-/-}$ compared with wild-type mice (Binder *et al*, 2004; Yao *et al*, 2008). Despite the increase of the extracellular space, the diffusional properties for large molecules was not different between these AQP4$^{-/-}$ and wild-type mice (Xiao and Hrabetova, 2009). The mdx and Syn$^{-/-}$ mice display baseline morphological abnormalities, including swollen astrocyte foot processes (Amiry-Moghaddam *et al*, 2004) and increased BBB permeability (Frigeri *et al*, 2001; Nico *et al*, 2003). However, these abnormalities did not alter MRI measurements in mdx mice, where brain ADC values were similar between mdx and wild-type mice (Vajda *et al*, 2002). In these murine models, deletion of dystrophin and syntrophin may affect other transporters and proteins with potential compensatory mechanisms inhibiting any observable changes in ADC values.

Until now, the contribution of astrocytic AQP4 in water diffusion has never been investigated directly *in vivo* in normal brain. *In vitro*, the water permeability of cells has been indirectly determined by measuring the kinetics and the maximum degree of astrocyte cell swelling in response to solution exchange between isotonic and hypotonic saline (Nicchia *et al*, 2003, 2005). Cell swelling is significantly reduced in astrocytes that did not express AQP4, suggesting that this water channel contributes significantly to astrocytic water movement *in vitro* (Nicchia *et al*, 2003, 2005). In our *in vitro* experiments, siAQP4 induced a significant decrease in AQP4 expression in primary mouse astrocyte cultures 3 days (Figure 2; Supplementary Figure 2) after application in accordance with previous studies (Nicchia *et al*, 2005; Saadoun *et al*, 2005). Decreased AQP4 expression did not alter the morphology of the astrocytes in our primary cultures (Figure 2), although the water permeability of the cells was significantly decreased (data not shown).

Similarly, cortical injection of siAQP4 induced a decrease in AQP4 at the site of injection and remotely in the contralateral striatum (Figure 4) after 3 days. The 27% decrease in AQP4 in the ipsilateral hemisphere did not affect astrocyte morphology based on GFAP analysis (Figure 6), similar to that observed *in vitro*. Thus, at 3 days, decreased AQP4 levels induced a significant decrease in ADC values without modification of tissue histology, BBB disruption, neuronal cell death nor significant modification of astrocyte morphology (Figures 5 and 6). Evaluation of ADC before 3 days did not reveal any decrements (Supplementary Figure 5A), consistent with the notion that a threshold reduction in AQP4 expression is needed to elicit the 50% reduction in ADC values reported in our studies. The decrements in AQP4 expression do not change brain water content (Supplementary Figure 5B). Together, our results in the normal brain revealed that AQP4 significantly contributes to ADC values, a measure of water diffusion. Previously, decreased ADC values have been related to a decrease in the extracellular space, as a consequence of cellular swelling under pathological conditions (Figure 1). Early decreases in ADC values in the hypoxic-ischemic rat model correlated with decreased AQP4 expression (Meng *et al*, 2004). In a rat model of hydrocephalus, an increased level of AQP4 expression correlated with increased ADC (Tourdias *et al*, 2009). Previous work in pathological conditions and our study in normal brain suggest that altered astrocyte water permeability likely has a critical role in water mobility. The contribution of astrocytic AQP4 to ADC values reinforces the importance of the astrocytic compartment in neuroimaging.

The needle induced a mild mechanical lesion with an increase in GFAP staining in the ipsilateral cortex and with BBB disruption (Figures 5 and 6). Interestingly, we observed that siAQP4 injection prevented the increase in GFAP and BBB disruption induced by the needle track (Figures 5 and 6). These observations suggest that injection of siAQP4 may prevent gliosis formation and BBB disruption induced by mechanical forces. Our results are in accordance with previous reports in AQP4$^{-/-}$ mice showing that the absence of AQP4 protects against cell death caused by edema (Manley *et al*, 2000; Saadoun *et al*, 2008) and inhibits glial scar formation (Auguste *et al*, 2007; Saadoun *et al*, 2005). Our results suggest a promising future for the use of siRNA therapies against AQP4. We speculate that this novel approach of AQP4 silencing could be used to prevent edema formation after acute brain injury, particularly with improved methods of drug delivery (e.g. intranasal route).

The cellular location of AQP4 in astrocytic endfeet in contact with cerebral blood vessels (Supplementary Figure 4) suggests a role in BBB modulation (Wolburg *et al*, 2009). AQP4$^{-/-}$ mice showed both disruption (Zhou *et al*, 2008) and no change of the BBB (Saadoun *et al*, 2009). In our experience, decreased AQP4 at sites distant from the injection site (contralateral striatum) did not alter BBB permeability (Figure 5C). In accordance with previous studies, our results demonstrate that decreased AQP4 does not induce leakage of the BBB (Saadoun *et al*, 2009). Our results are consistent with the idea that AQP4 is not critical for BBB maintenance in normal brain, in the absence of mechanical or metabolic stress.

In conclusion, involvement of AQP4 in modulating ADC values strengthens the role of the neurovascular unit in regulating water movement under normal and pathological conditions, where decreased ADC values are usually interpreted as reflective of cytotoxic edema, which may be due to decreased AQP4 expression. The contribution of

astrocytic AQP4 to ADC values reinforces the importance of the astrocytic compartment in neuroimaging.

## Acknowledgements

The authors thank Dr JF Brunet for his help for *in vitro* experiments and Dr M Price for her critical reading of the manuscript.

## Disclosure/conflict of interest

The authors declare no conflict of interest.

## References

Amiry-Moghaddam M, Otsuka T, Hurn PD, Traystman RJ, Haug F-M, Froehner SC, Adams ME, Neely JD, Agre P, Ottersen OP, Bhardwaj A (2003) An alpha-syntrophin-dependent pool of AQP4 in astroglial end-feet confers bidirectional water flow between blood and brain. *PNAS* 100:2106–11

Amiry-Moghaddam M, Xue R, Haug FM, Neely JD, Bhardwaj A, Agre P, Adams ME, Froehner SC, Mori S, Ottersen OP (2004) Alpha syntrophin deletion removes the perivascular but not the endothelial pool of aquaporin-4 at the blood-brain barrier and delays the development of brain edema in an experimental model of acute hyponatremia. *FASEB J* 18:542–4

Auguste KI, Jin S, Uchida K, Yan D, Manley GT, Papadopoulos MC, Verkman AS (2007) Greatly impaired migration of implanted aquaporin-4-deficient astroglial cells in mouse brain toward a site of injury. *FASEB J* 21:108–16

Badaut J, Ashwal S, Tone B, Regli L, Tian HR, Obenaus A (2007) Temporal and regional evolution of aquaporin-4 expression and magnetic resonance imaging in a rat pup model of neonatal stroke. *Pediatr Res* 62:248–54

Badaut J, Hirt L, Price M, de Castro Ribeiro M, Magistretti PJ, Regli L (2005) Hypoxia/hypoglycemia preconditioning prevents the loss of functional electrical activity in organotypic slice cultures. *Brain Res* 1051:117–22

Badaut J, Lasbennes F, Magistretti PJ, Regli L (2002) Aquaporins in brain: distribution, physiology, and pathophysiology. *J Cereb Blood Flow Metab* 22:367–78

Binder DK, Papadopoulos MC, Haggie PM, Verkman AS (2004) *In vivo* measurement of brain extracellular space diffusion by cortical surface photobleaching. *J Neurosci* 24:8049–56

Brunet JF, Grollimund L, Chatton JY, Lengacher S, Magistretti PJ, Villemure JG, Pellerin L (2004) Early acquisition of typical metabolic features upon differentiation of mouse neural stem cells into astrocytes. *Glia* 46:8–17

de Castro Ribeiro M, Hirt L, Bogousslavsky J, Regli L, Badaut J (2006) Time course of aquaporin expression after transient focal cerebral ischemia in mice. *J Neurosci Res* 83:1231–40

Frigeri A, Nicchia GP, Nico B, Quondamatteo F, Herken R, Roncali L, Svelto M (2001) Aquaporin-4 deficiency in skeletal muscle and brain of dystrophic mdx mice. *FASEB J* 15:90–8

Hirt L, Badaut J, Thevenet J, Granziera C, Regli L, Maurer F, Bonny C, Bogousslavsky J (2004) D-JNKI1, a cell-penetrating c-Jun-N-terminal kinase inhibitor, protects against cell death in severe cerebral ischemia. *Stroke* 35:1738–43

Hirt L, Price M, Ternon B, Mastour N, Brunet JF, Badaut J (2009) Early induction of AQP4 contributes the limitation of the edema formation in the brain ischemia. *J Cereb Blood Flow Metab* 29:423–33

Le Bihan D (2007) The 'wet mind': water and functional neuroimaging. *Phys Med Biol* 52:R57–90

Manley GT, Binder DK, Papadopoulos MC, Verkman AS (2004) New insights into water transport and edema in the central nervous system from phenotype analysis of aquaporin-4 null mice. *Neuroscience* 129:981–9

Manley GT, Fujimura M, Ma T, Noshita N, Filiz F, Bollen AW, Chan P, Verkman AS (2000) Aquaporin-4 deletion in mice reduces brain edema after acute water intoxication and ischemic stroke. *Nat Med* 6:159–63

Meng S, Qiao M, Lin L, Del Bigio MR, Tomanek B, Tuor UI (2004) Correspondence of AQP4 expression and hypoxic-ischaemic brain oedema monitored by magnetic resonance imaging in the immature and juvenile rat. *Eur J Neurosci* 19:2261–9

Nicchia GP, Frigeri A, Liuzzi GM, Svelto M (2003) Inhibition of aquaporin-4 expression in astrocytes by RNAi determines alteration in cell morphology, growth, and water transport and induces changes in ischemia-related genes. *FASEB J* 17:1508–10

Nicchia GP, Srinivas M, Li W, Brosnan CF, Frigeri A, Spray DC (2005) New possible roles for aquaporin-4 in astrocytes: cell cytoskeleton and functional relationship with connexin43. *FASEB J* 19:1674–6

Nico B, Frigeri A, Nicchia GP, Corsi P, Ribatti D, Quondamatteo F, Herken R, Girolamo F, Marzullo A, Svelto M, Roncali L (2003) Severe alterations of endothelial and glial cells in the blood-brain barrier of dystrophic mdx mice. *Glia* 42:235–51

Obenaus A, Ashwal S (2008) Magnetic resonance imaging in cerebral ischemia: focus on neonates. *Neuropharmacology* 55:271–80

Obenaus A, Robbins M, Blanco G, Galloway NR, Snissarenko E, Gillard E, Lee S, Curras-Collazo M (2007) Multimodal magnetic resonance imaging alterations in two rat models of mild neurotrauma. *J Neurotrauma* 24:1147–60

Papadopoulos MC, Manley GT, Krishna S, Verkman AS (2004) Aquaporin-4 facilitates reabsorption of excess fluid in vasogenic brain edema. *FASEB J* 18:1291–3

Saadoun S, Bell BA, Verkman AS, Papadopoulos MC (2008) Greatly improved neurological outcome after spinal cord compression injury in AQP4-deficient mice. *Brain* 131:1087–98

Saadoun S, Papadopoulos MC, Watanabe H, Yan D, Manley GT, Verkman AS (2005) Involvement of aquaporin-4 in astroglial cell migration and glial scar formation. *J Cell Sci* 118:5691–8

Saadoun S, Tait MJ, Reza A, Davies DC, Bell BA, Verkman AS, Papadopoulos MC (2009) AQP4 gene deletion in mice does not alter blood-brain barrier integrity or brain morphology. *Neuroscience* 161:764–72

Soltys Z, Orzylowska-Sliwinska O, Zaremba M, Orlowski D, Piechota M, Fiedorowicz A, Janeczko K, Oderfeld-Nowak B (2005) Quantitative morphological study of microglial cells in the ischemic rat brain using principal component analysis. *J Neurosci Methods* 146:50–60

Tait MJ, Saadoun S, Bell BA, Papadopoulos MC (2008) Water movements in the brain: role of aquaporins. *Trends Neurosci* 31:37–43

Tourdias T, Dragonu I, Fushimi Y, Deloire MS, Boiziau C, Brochet B, Moonen C, Petry KG, Dousset V (2009) Aquaporin 4 correlates with apparent diffusion coefficient and hydrocephalus severity in the rat brain: a combined MRI-histological study. *Neuroimage* 47: 659–66

Vajda Z, Pedersen M, Fuchtbauer EM, Wertz K, Stodkilde-Jorgensen H, Sulyok E, Doczi T, Neely JD, Agre P, Frokiaer J, Nielsen S (2002) Delayed onset of brain edema and mislocalization of aquaporin-4 in dystrophin-null transgenic mice. *Proc Natl Acad Sci USA* 99:13131–6

Wolburg H, Noell S, Wolburg-Buchholz K, Mack A, Fallier-Becker P (2009) Agrin, aquaporin-4, and astrocyte polarity as an important feature of the blood-brain barrier. *Neuroscientist* 15:180–93

Xiao F, Hrabetova S (2009) Enlarged extracellular space of aquaporin-4-deficient mice does not enhance diffusion of Alexa Fluor 488 or dextran polymers. *Neuroscience* 161:39–45

Yao X, Hrabetova S, Nicholson C, Manley GT (2008) Aquaporin-4-deficient mice have increased extracellular space without tortuosity change. *J Neurosci* 28: 5460–4

Zhou J, Kong H, Hua X, Xiao M, Ding J, Hu G (2008) Altered blood-brain barrier integrity in adult aquaporin-4 knockout mice. *Neuroreport* 19:1–5

Supplementary Information accompanies the paper on the Journal of Cerebral Blood Flow & Metabolism website (http://www.nature.com/jcbfm)